ACS Sustainable Resource Management

pubs.acs.org/acssrm

Article

Generic Proton Binding Parameters of a Three-Site NICA-Donnan Model for Plant-Based Biochars

Yifan Huang, Gerwin F. Koopmans, Jan E. Groenenberg, Zhengguo Song, Liping Weng,* and Rob N. J. Comans

Cite This: *ACS Sustainable Resour. Manage.* 2024, 1, 707−720

Read Online

ACCESS | Metrics & More | Article Recommendations | Supporting Information

ABSTRACT: The charging behavior of biochars resulting from (de)protonation is important for assessing their potential as adsorbents for *in situ* immobilization of trace metals in polluted soils. Here, the pH-charge curves of 20 newly produced biochars were measured, whereas curves of 16 other biochars were collected from literature. All 36 biochars were produced from different plant-based materials at various pyrolysis temperatures. The pH-charging data were used to derive proton binding parameters for a novel three-site NICA-Donnan model, accounting for proton binding to carboxylic ($site_{a1}$) and phenolic ($site_{a2}$) acidic groups as well as to a basic ($site_b$) group. This model successfully described the proton binding behavior of the 36 biochars at different ionic strengths for the first time, by extending the classical two-site NICA model with a basic group in combination with an electrostatic Donnan model using a fixed volume of 0.1 L kg^{-1}. A set of generic proton binding parameters derived from the data resulted in a relative error of ∼6% for proton adsorption by all 36 biochars. Recommended parameters are Q_{a1} = 0.39 mol kg^{-1}, log $\tilde{K}_{a1}$ = 4.55, m_{a1} = 0.70, Q_{a2} = 0.59 mol kg^{-1}, log $\tilde{K}_{a2}$ = 8.10, m_{a2} = 0.80, Q_b = 0.39 mol kg^{-1}, log $\tilde{K}_b$ = 4.78, and m_b = 0.76.

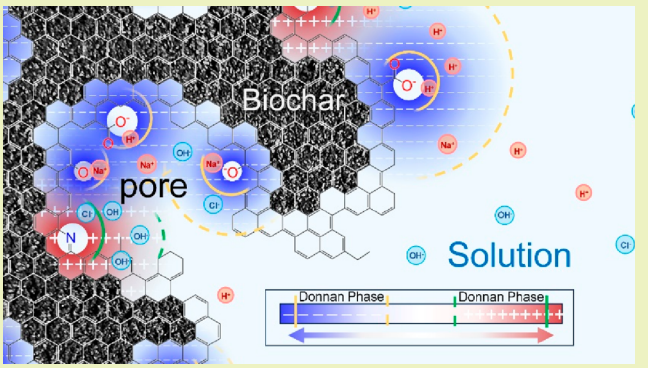

KEYWORDS: *Biochar, Functional groups, Proton binding, NICA-Donnan model*

1. INTRODUCTION

Biochar is a carbon-rich material derived from pyrolysis of biomass under oxygen-limited conditions,[1] serving various purposes like air purification, water treatment,[2] and soil remediation.[3,4] Biochar amendment of trace metal-polluted soils will increase the adsorption of trace metals when the soil binding capacity is limited, decreasing their equilibrium concentration in soil solution[5] and reducing their accumulation in crops and leaching.[6,7] Using biochar as a soil amendment in soil remediation operations to reduce environmental risks of polluted soils is more sustainable than conventional remediation techniques[8,9] because biochar application contributes, for example, to the improvement of important soil functions like carbon sequestration to mitigate global warming and water and nutrient retention in support of soil fertility and agricultural production.[10] Most biochars are produced from plant-based materials like straw and wood,[11,12] which are composed of polysaccharides (cellulose and hemicellulose) and polyphenols (lignin),[13] at a pyrolysis temperature usually varying between 300 and 600°C.[14] Differences in plant biomass composition and pyrolysis temperature influence biochar properties including their carbon content, aromaticity, porosity, surface area, and type and density of surface functional groups.[1,15] Since these properties affect proton and trace metal binding by biochars, it is crucial to assess their capacity and affinity to bind trace metals over a wide range in soil properties including pH and ionic strength in the presence of other competing/synergistic ions when selecting an appropriate biochar for *in situ* soil remediation. This can be done in standardized laboratory experiments using soil batch experiments,[16] although this approach is laborious because the effects of many combinations of different soil properties must be investigated. Alternatively, surface complexation models (SCM) can be used to obtain a quantitative insight in the capability of biochars to bind trace metals over a wide range of relevant soil properties.[17,18] Determining the charging behavior of variable charge adsorbents like biochar as a function of pH and ionic strength through potentiometric acid−base titrations and modeling of the protonation reactions are the first steps to identify the types and densities of reactive groups,[19−21] laying the basis for further model development including a

Received: November 17, 2023
Revised: February 29, 2024
Accepted: March 13, 2024
Published: March 28, 2024

quantitative description of trace metal adsorption. The non-ideal competitive consistent adsorption-Donnan (NICA-Donnan) model is an advanced SCM used for calculating ion binding to humic substances including humic acids (HA) and fulvic acids (FA).[19,22,23] The NICA model describes the intrinsic heterogeneity of carboxylic- and phenolic-type reactive groups for ion binding to humic substances, with each group having its own continuous affinity distribution,[19] whereas the Donnan model accounts for electrostatic interactions.[22] Deriving generic NICA-Donnan parameters from extensive datasets of ion binding to HA and FA[24,25] has enabled the successful prediction of pH-dependent trace metal binding to humic substances in batch systems with FA and/or HA as well as in various natural soils and aquatic ecosystems.[26−33]

Similar to humic substances, biochars have a complex aromatic skeleton with carboxylic and phenolic groups,[34,35] exhibiting intrinsic heterogeneity for ion binding. However, the charging behavior of both materials is different. Humic substances are generally negatively charged in the natural soil pH range.[24] In contrast, biochars have a net positive charge in an acidic environment and a net negative charge in a basic environment, as they mostly have a point of zero charge (PZC) in the pH range of ∼6−8.[36−38] This charging behavior of biochars has been attributed to the presence of acidic as well as basic groups.[39,40] Carboxylic- and phenolic-type groups have been identified as the acidic functional groups of biochar, whereas the basic group can be attributed to N-containing heterocyclic structures such as pyridine and graphitic-N.[34,35] For describing the acid−base behavior of a series of plant-based biochars produced at different pyrolysis temperatures, Li et al.[39] used a discrete heterogeneous site-binding model with two acidic groups and one basic group. More recently, Xiong et al.[21] successfully extended the classical two-site NICA model with a basic group to describe the chemical heterogeneity of two washed plant-based biochars in proton adsorption. Yet another difference between humic substances and biochar is the bulk structure of the materials. Both biochars and humic substances normally have a residual net charge (except at the PZC of biochars), which is neutralized by electrostatic attraction of counterions and exclusion of co-ions.[41,42] Since humic substances are "soft" matter,[43] which can be interpreted as an open gel-like phase with a smeared-out charge distribution, a Donnan model approach can be used to describe electrostatic interactions in the gel.[41,42] Although the Donnan model was successfully used to describe ionic strength effects on proton binding by humic substances,[24] its applicability to small humic substances has been criticized.[44] In contrast to humic substances, biochars consist of porous solid material.[45] Although ionic strength had an impact on proton binding to biochars, Xiong et al.[21] did not use an electrostatic model to describe these electrostatic effects. Without an electrostatic model, the proton affinity parameters of their NICA model should be considered as conditional constants rather than intrinsic parameters.[21] However, application of electrostatic models to porous solid materials like biochars is challenging.

For porous hydrous ferric oxide aggregates, a Donnan model approach has been used for describing electrostatic interactions in intra-particle pores.[46] When diffuse layers in pores overlap as the Debye length is comparable to the pore diameter, it is appropriate to assume a constant charge and electrostatic potential inside the pore space and to use a Donnan model approach,[47] similar to humic substances. Here we test a Donnan model approach to account for electrostatic effects on proton binding by biochars, although not all biochar pores reported in literature justify the assumption of overlapping diffuse layers. For example, pores of rice straw-based biochars are mesoporous (2−50 nm),[48] whereas most pores in biochars produced from wood, chicken manure, and water hyacinth have a diameter <10 nm.[49] From our interpretation of data from Huang et al.,[49] the internal surface area of their biochars largely comes from pores <5 nm, comparable to the Debye length at an ionic strength of 0.01 M NaCl (∼3 nm). Despite the variation in reported pore size distributions of biochars, combining the three-site NICA model with the Donnan model is a step forward in describing proton adsorption to biochars as it facilitates the derivation of intrinsic proton affinity parameters for the NICA model.

We quantified proton adsorption by 20 biochars, produced from cellulose and lignin mixed at different ratios and maize straw and pine shaves at pyrolysis temperatures between 300−600°C using potentiometric acid−base titrations at three ionic strengths. Furthermore, we digitized pH-charge density curves of 16 other plant-based biochars from literature.[21,39] Our aim is to derive generic binding parameters for proton adsorption to biochars using a three-site NICA model combined with the Donnan model. We characterized selected biochars using a suite of spectroscopic techniques including NMR, XPS, and FTIR to validate the presence of the three reactive groups considered in the model. Finally, we compared the performance of the recommended generic parameters for describing proton binding to the 36 biochars against two alternative scenarios, *i.e.*, one scenario with biochar-specific site density (Q_{max}) values but generic binding affinity (log $\tilde{K}$) and heterogeneity (m) values and another scenario with only biochar-specific parameters. This scenario analysis will guide readers in their choice to use either generic parameters or experimentally derive some or even all of the parameters when modeling proton binding to a specific plant-based biochar.

2. METHODOLOGY

2.1. Biochar Preparation. Twenty biochars were produced from three mixtures of pure cellulose and lignin (mass ratio of 9:1, 7:3, and 6:4) and two raw materials including maize straw (MS) and pinewood shaves (PS) using four pyrolysis temperatures of 300, 400, 500, and 600 °C (Table S1). Powdered cellulose (99.9 wt %, CAS: 9004-34-6) and lignin (99.9 wt %, CAS: 8068-05-1) were purchased from HWRK Chemical Co., Ltd, China. The MS was collected near the city of Tianjin, China, whereas the PS was purchased from a commercial webshop (Deying Factory Shop, China). The MS and PS were oven-dried at 60°C and ground to <0.85 mm. Next, 50 g of these materials was put in a corundum crucible and placed in a sealed muffle furnace. After 2 h of N_2-flushing, the furnace was heated to 60°C within 30 min, followed by a 30 min-heating step to realize the desired pyrolysis temperature of either 300, 400, 500, or 600°C for 2 h.[50] The resulting biochars were carefully cleaned by two washings with 200 mL 6 M HCl and one washing with 200 mL 50% (v:v) ethanol, followed by washing with ultrapure water (Millipore) to remove impurities like $CaCO_3$ and SiO_2 and soluble organic matter,[51] and these impurities, if not removed, may react with protons thus influencing determination of charge of biochars. The washing with ultrapure water was repeated until the leachate conductivity was <0.5 μS cm^{-1}. The use of HCl to wash biochar effectively removes soluble organic matter.[52] The biochars were dried in a vacuum oven at 60°C until constant weight and stored in polypropylene tubes (Corning).

2.2. Acid−Base Titrations and Spectroscopic Characterization. Acid−base titrations were used to quantify the charging

https://doi.org/10.1021/acssusresmgt.3c00104
ACS Sustainable Resour. Manage. 2024, 1, 707−720

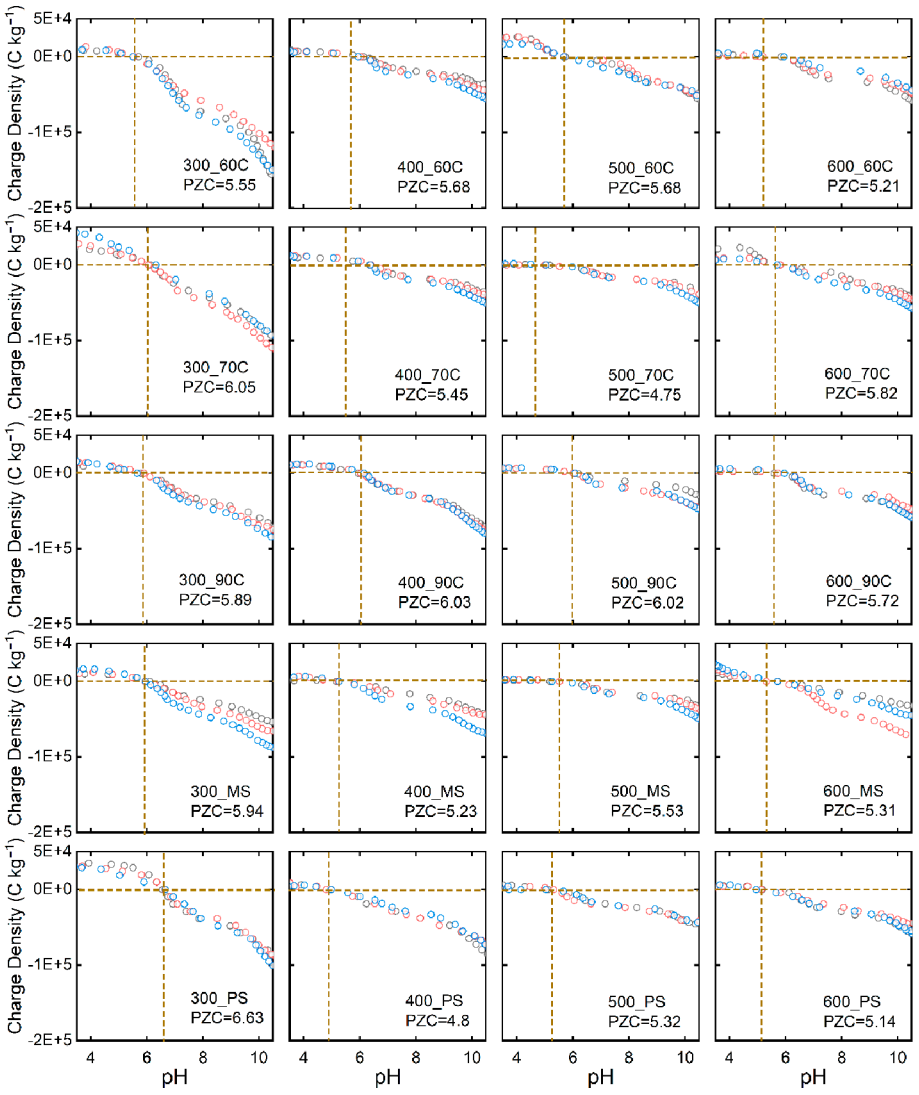

Figure 1. Experimental pH-charge density curves of the 20 biochars produced in this study measured at an ionic strength of 0.01 M (black circles), 0.05 M (red circles), and 0.1 M NaCl (blue circles). The horizonal dashed line is the zero-charge line, whereas the vertical dashed line indicates the point of zero charge (PZC).

behavior of the 20 newly-produced biochars as a function of pH (pH 3.5−10.5) at three ionic strengths of 0.01, 0.05, and 0.1 M imposed by NaCl. The details of the experimental procedure are described in SI-1. We used cross-polarization magic-angle spinning solid ^{13}C nuclear magnetic resonance (NMR) spectroscopy, X-ray photoelectron spectroscopy (XPS), and Fourier-transform infrared spectroscopy (FTIR) to identify surface functional groups of selected biochars. Details of these techniques are given in SI-2.

2.3. Literature Data. The pH-charge density curves of 14 plant-based biochars from Li et al.[39] and 2 biochars from Xiong et al.[21] were used to complement our dataset (Table S1). The biochars of Li et al.[39] were produced from two aquatic plant species (*Spartina alterniflora* (SA) and *Eichhornia crassipes* (WH)) at pyrolysis temperatures between 60−700°C,[39] whereas the biochars of Xiong et al.[21] were prepared from pinewood chips (WB) and palm silk (PB) at a pyrolysis temperature of 400 and 600°C.[21] Biochars from both studies were cleaned by washing with NaOH and HCl, followed by rinsing with water and air drying (Table S1). Washing is important because impurities like salts and soluble organic matter[51] have to be removed from biochar as they consume protons and influence acid−base titration results. However, an adequate description of the washing procedure is often lacking in acid−base titration studies with biochar reported in literature, hindering the use of the pH-charging data. The datasets of Li et al.[39] and Xiong et al.[21] were selected here, because, as in our study, they included HCl for biochar washing, which is effective in removing inorganic minerals.[53] Furthermore, additional data of 169 other plant-based biochars were collected to investigate the effects of the washing procedure and pyrolysis temperature on the PZC of biochar (SI-3, Table S2).

2.4. Three-Site NICA-Donnan Model. We adopted the three-site NICA model (eq 1) with two acidic groups and one basic group from Xiong et al.[21] to describe proton binding to the 20 newly-produced biochars and the 16 biochars collected from literature[21,39] (Table S1):

$$Q_{\mathbf{H}} = Q_{\mathbf{max,a1}} \times \frac{(\tilde{K}_{\mathbf{a1}} \times [\mathbf{H_D}])^{m_{\mathbf{a1}}}}{1 + (\tilde{K}_{\mathbf{a1}} \times [\mathbf{H_D}])^{m_{\mathbf{a1}}}} + Q_{\mathbf{max,a2}} \times \frac{(\tilde{K}_{\mathbf{a2}} \times [\mathbf{H_D}])^{m_{\mathbf{a2}}}}{1 + (\tilde{K}_{\mathbf{a2}} \times [\mathbf{H_D}])^{m_{\mathbf{a2}}}} + Q_{\mathbf{max,b}} \times \frac{(\tilde{K}_{\mathbf{b}} \times [\mathbf{H_D}])^{m_{\mathbf{b}}}}{1 + (\tilde{K}_{\mathbf{b}} \times [\mathbf{H_D}])^{m_{\mathbf{b}}}} \quad (1)$$

where Q_H is the amount of protons bound (mol kg^{-1}); the subscript *ai* refers to the acidic binding sites with *i* being either acidic site 1 (carboxylic-type groups) or acidic site 2 (phenolic-type groups); the subscript b refers to the basic site; $Q_{max,ai}$ and $Q_{max,b}$ represent the binding site density of each reactive group (mol kg^{-1}); log $\tilde{K}_{ai}$ and log $\tilde{K}_b$ are the median values of the proton affinity distribution for each

https://doi.org/10.1021/acssusresmgt.3c00104
ACS Sustainable Resour. Manage. 2024, 1, 707−720

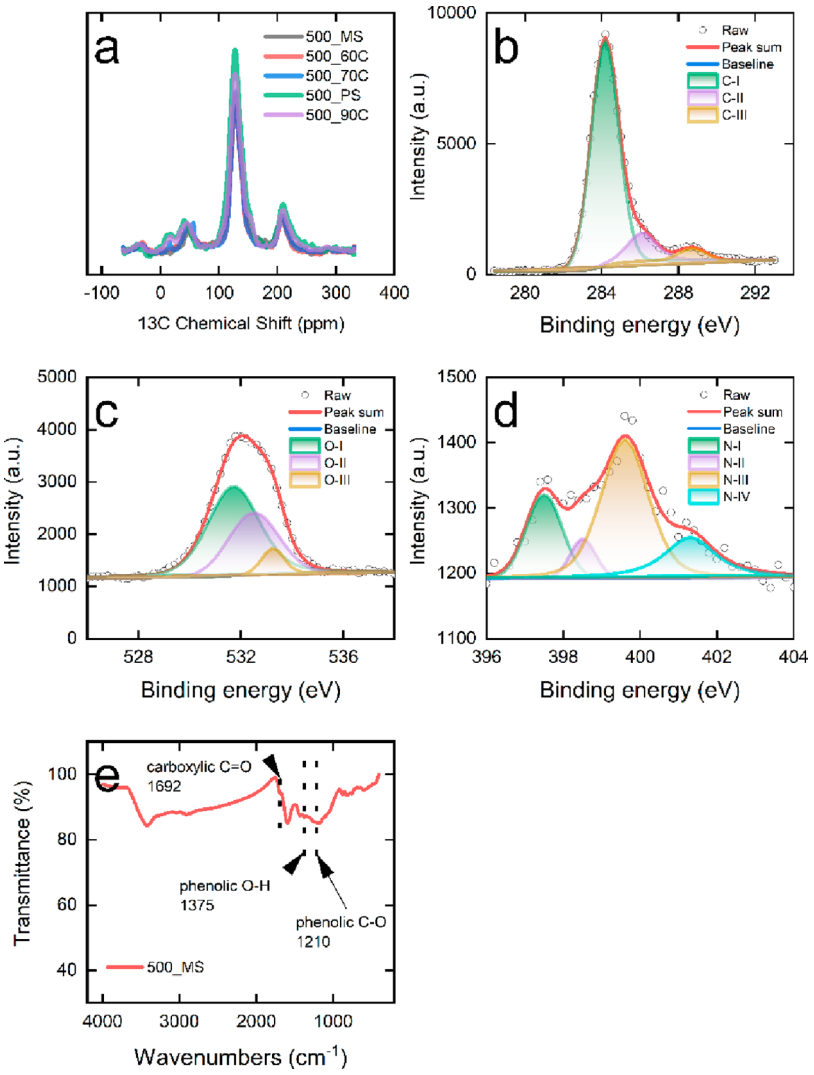

Figure 2. Spectroscopic analysis of biochars. Figure 2a: ^{13}C NMR spectra of five selected biochars produced in this study at a pyrolysis temperature of 500°C (500_60C, 500_70C, 500_90C, 500_MS, and 500_PS). In Figure 2b–d: Results of the XPS analysis of the 500_MS biochar, with deconvolution of carbon (2b), oxygen (2c), and nitrogen (2d). Figure 2e: FTIR spectrum of the 500_MS biochar.

group; $[H_D]$ is the local proton concentration in the Donnan phase; and m_{ai} and m_b reflect the apparent binding site heterogeneity.

We used a Donnan model with a constant V_D to describe the electrostatic effects on proton binding by biochar. This is in contrast to "soft" humic substances for which V_D depends on ionic strength to reflect their shrinking and swelling behavior.[42,54] The Donnan potential (Ψ_D) can be calculated, describing the electrostatic potential difference between the adsorbent phase and the aqueous bulk phase based on the charge density of biochar at a given pH and ionic strength.[22] Once Ψ_D is known, $[H_D]$ can be calculated from the product of the Boltzmann factor B, which includes Ψ_D, and the proton activity in the aqueous bulk phase (H_{aq}), *i.e.*, $[H_D] = B(H_{aq})$.[22] Subsequently, proton binding can be calculated on the basis of $[H_D]$ rather than (H_{aq}). Consequently, the proton binding affinity parameters $\log\tilde{K}$ no longer depend on ionic strength and can be considered as non-conditional and intrinsic parameters,[54,55] enabling us to describe the pH-charge density curves measured at different ionic strengths using one set of model parameters. For optimizing the three-site NICA-Donnan model parameters, we followed the steps described in SI-4 and SI-5 using the parameter estimation software FIT (version 2.581)[56] as implemented in the chemical speciation software ECOSAT (version 4.9).[57]

3. RESULTS AND DISCUSSION

3.1. Point of Zero Charge. The pH-charge density curves of the 20 newly-produced biochars measured at the three ionic strengths of 0.01, 0.05, and 0.1 M are presented in Figure 1. They have a PZC between pH 4.8–6.6, which can be explained by the presence of both acidic and basic groups.[58,59] We characterized the surface functional groups of selected biochars using ^{13}C NMR, XPS, and FTIR. These biochars are highly aromatized and contain carboxylic and phenolic groups and basic groups like N-containing heterocyclic structures (*i.e.*, pyridine and graphitic-N) (see SI-2, Table S3, Figure 2), providing experimental evidence for the presence of two acidic groups and a basic group in the three-site NICA model. In addition to the 36 biochars used here, we collected PZC data of 169 other plant-based biochars from literature (Table S2). The PZC of all 205 biochars varies widely from 1.00 to 12.43 with an average of 7.46 (Figure 3). Multiple factors like raw material type, pyrolysis temperature, and washing method are likely to contribute to the variation in PZC.[60] No significant differences were detected between the average PZC of the biochars grouped by washing method (see SI-3, Figure S1), although using acid or base to wash biochars can potentially

https://doi.org/10.1021/acssusresmgt.3c00104
ACS Sustainable Resour. Manage. 2024, 1, 707–720

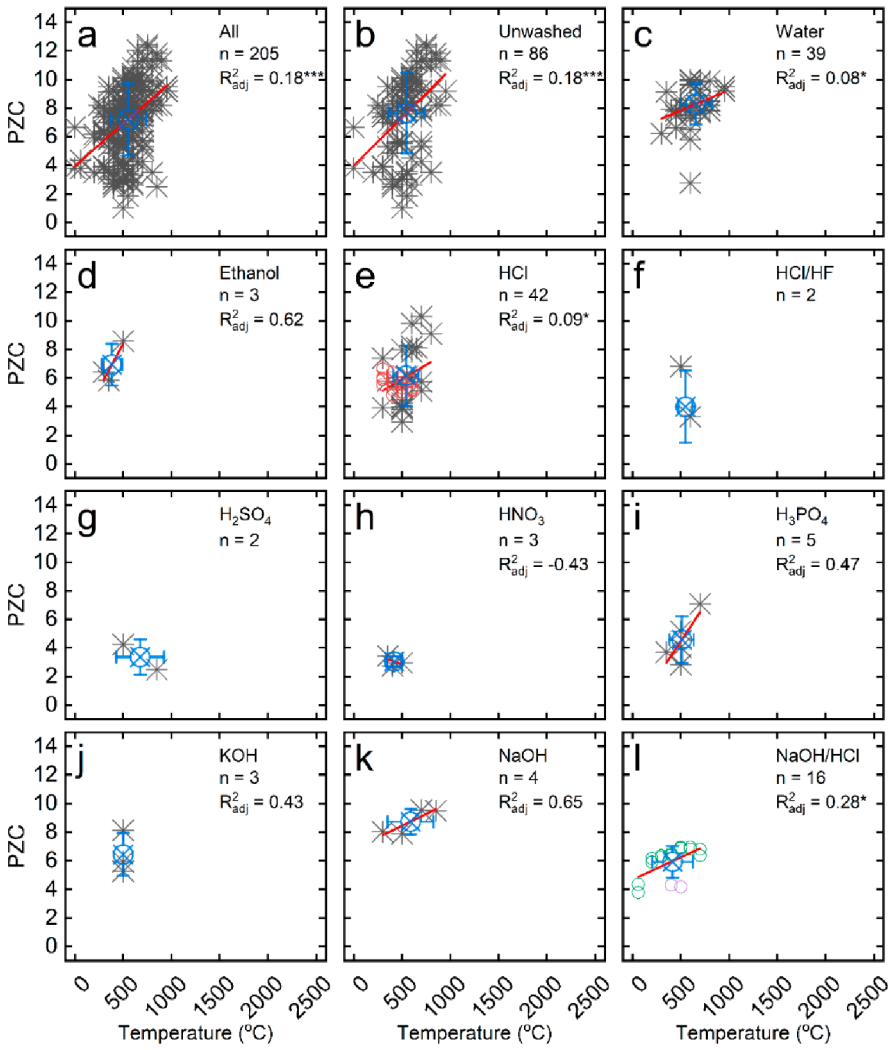

Figure 3. Relationships between the point of zero charge (PZC) and pyrolysis temperature for all biochars, all unwashed biochars, and biochars grouped according to the washing method (*n* represents the number of biochars). The blue circle with error bar represents the mean PZC and mean pyrolysis temperature of the grouped biochars, whereas the red solid lines represent the results of the linear regression analysis including the R^2_{adj} and the level of significance. The level of significance was expressed using * for $p < 0.05$ and *** for $p < 0.001$. The red circles (○) in Figure 3e represent the PZC of the 20 biochars produced in this study, whereas the green circles (○) and the purple circles (○) in Figure 3l represent the 16 biochars taken from Li et al.[39] and Xiong et al.,[21] respectively.

alter the type and content of surface functional groups by chemical oxidation and hydrolysis, as has been shown for humic substances.[61−64] For all biochars (including unwashed biochars and biochars washed with different solutions), the PZC increased linearly with pyrolysis temperature ($p < 0.001$, Figure 3). Likewise, a positive linear relation was found for biochars washed either with water, HCl, or NaOH/HCl ($p < 0.05$). Pyrolysis temperature affects the ash content, aromaticity, and the type and site density of surface functional groups of biochars,[65] which can influence the PZC. This is supported by the decrease in the density of carboxylic-type groups of the 36 biochars with pyrolysis temperature (see Section 3.3).

3.2. Charging Behaviour. When the pH is <PZC, our 20 newly-produced biochars have a net weak positive charge, whereas they have a net negative charge when the pH is >PZC (Figure 1). Since the biochars have a net positive charge below their PZC with the carboxylic-type groups being partly deprotonated and thus providing negative charge, they must contain basic groups to overcompensate for this negative charge. Indeed, this corresponds with our results from the spectroscopic biochar characterization (see SI-2, Figure 2). Our findings on the biochar charging behavior are consistent with earlier observations.[21,39] The charge density of our 20 newly produced biochars ranges from 2.63×10^4 to -1.30×10^5 C kg^{-1} at pH 4 to 10, whereas this range is from 3.99×10^3 to -1.73×10^5 C kg^{-1} and 1.43×10^3 to -3.09×10^5 C kg^{-1} for biochars from Li et al.[39] and Xiong et al.,[21] respectively. The net positive charge of biochars below their PZC contrasts with humic substances,[24] which are negatively charged in the natural soil pH range of 4-10. Biochar has a lower charge density than humic substances. For example, the charge density of humic substances varies between -2.7×10^5 and -6.8×10^5 C kg^{-1} at pH 9,[24] whereas it is between -1.18×10^4 and -1.51×10^5 C kg^{-1} at the same pH for the 36 biochars studied here. Furthermore, the ionic strength effect on the charge density of biochars is greater than for humic substances when the pH is >PZC, whereas it is weaker when the pH is <PZC. This weaker ionic strength effect is the result of the limited pH range when pH is <PZC. For example, the average charge

https://doi.org/10.1021/acssusresmgt.3c00104
ACS Sustainable Resour. Manage. 2024, 1, 707−720

Table 1. Proton Binding Parameters of the Three-Site NICA-Donnan Model Derived for the 20 biochars Produced in This Study and the 16 Other Biochars from Li et al.[39] and Xiong et al.[21a]

Biochar	$Q_{max,a1}$ (mol kg^{-1})	$Q_{max,a2}$ (mol kg^{-1})	$Q_{max,b}$ (mol kg^{-1})	log $\tilde{K}_{a1}$	log $\tilde{K}_{a2}$	log $\tilde{K}_{b}$	m_{a1}	m_{a2}	m_b[c]	R^2	$RMSE_1$ (mol kg^{-1})	$RMSE_2$ (mol kg^{-1})	$RMSE_3$ (mol kg^{-1})
300_90C	0.47	0.60	0.58	4.43	7.92	4.64	0.73	0.98	0.92	0.96	0.35	0.06	0.06
300_MS	0.33	0.51	0.38	4.37	6.93	4.69	0.55	0.78	0.92	0.97	0.08	0.11	0.07
300_70C	0.42	0.85	0.72	3.32	7.90	5.08	0.52	0.98	0.77	0.57	0.36	0.45	0.29
300_PS	0.48	0.53	0.72	5.34	7.46	5.75	0.55	0.98	0.92	0.86	0.42	0.40	0.17
300_60C	0.52	0.89	0.53	3.16	9.53	6.99	0.55	0.73	0.78	0.21	0.52	0.57	0.42
400_90C	0.39	0.76	0.44	4.20	8.06	5.03	0.55	0.98	0.95	0.95	0.07	0.07	0.07
400_MS	0.24	0.28	0.30	4.21	6.96	4.54	0.59	0.79	0.86	0.91	0.09	0.11	0.07
400_70C	0.23	0.33	0.35	4.61	8.11	5.28	0.55	0.98	0.85	0.95	0.17	0.05	0.05
400_PS	0.43	0.85	0.44	3.75	8.55	4.56	0.52	0.67	0.63	0.91	0.09	0.11	0.09
400_60C	0.19	0.45	0.28	3.59	7.89	4.78	0.55	0.95	0.98	0.96	0.13	0.05	0.04
500_90C	0.25	0.45	0.26	4.61	8.67	5.35	0.55	0.95	0.89	0.97	0.17	0.07	0.03
500_MS	0.21	0.26	0.24	3.65	9.01	5.20	0.91	0.83	0.61	0.96	0.19	0.04	0.03
500_70C	0.21	0.60	0.11	4.41	8.62	5.20	0.55	0.95	0.98	0.99	0.23	0.13	0.02
500_PS	0.26	0.24	0.31	3.01	7.46	4.67	0.83	0.92	0.98	0.94	0.11	0.06	0.04
500_60C	0.39	0.25	0.41	5.78	8.22	5.81	0.95	0.92	0.98	0.89	0.14	0.12	0.09
600_90C	0.34	0.22	0.37	3.60	7.68	5.04	0.82	0.93	0.88	0.90	0.12	0.07	0.07
600_MS	0.43	0.92	0.43	4.99	7.88	4.94	0.95	0.68	0.87	0.84	0.13	0.15	0.11
600_70C	0.16	0.46	0.23	4.19	7.57	5.89	0.95	0.71	0.78	0.82	0.13	0.10	0.08
600_PS	0.26	0.48	0.35	4.21	8.03	5.25	0.95	0.66	0.69	0.90	0.11	0.08	0.07
600_60C	0.25	0.41	0.22	4.28	8.12	4.76	0.95	0.71	0.86	0.83	0.13	0.08	0.08
60_SA	0.41	0.81	0.25	2.81	7.58	2.67	0.74	0.43	0.47	1.00	0.23	0.18	0.02
60_WH	1.08	0.81	0.45	6.71	8.84	8.91	0.86	0.68	0.66	1.00	0.18	0.76	0.03
200_SA	0.58	0.62	0.28	5.90	8.13	3.91	0.65	0.69	0.89	1.00	0.10	0.10	0.01
200_WH	0.88	0.90	0.49	6.93	10.34	3.70	0.71	0.76	0.74	0.98	0.09	0.49	0.04
300_SA	0.53	0.64	0.29	5.71	8.15	4.11	0.63	0.74	0.59	1.00	0.08	0.08	0.01
300_WH	0.74	0.99	0.50	7.14	9.17	4.28	0.71	0.76	0.71	1.00	0.12	0.43	0.02
400_SA	0.47	0.69	0.30	3.96	7.92	5.13	0.63	0.76	0.59	0.99	0.10	0.04	0.03
400_WH	0.66	1.06	0.51	6.26	9.31	3.16	0.63	0.74	0.76	0.99	0.05	0.30	0.03
500_SA	0.27	0.50	0.35	3.20	6.31	3.32	0.57	0.76	0.59	0.98	0.13	0.22	0.07
500_WH	0.42	0.93	0.55	4.35	8.50	4.62	0.62	0.77	0.67	0.95	0.06	0.09	0.02
600_SA	0.32	0.61	0.39	3.85	6.95	3.20	0.72	0.65	0.59	1.00	0.13	0.17	0.03
600_WH	0.54	0.91	0.64	4.87	8.90	5.02	0.74	0.79	0.64	0.99	0.06	0.17	0.02
700_SA	0.48	0.62	0.40	5.67	8.10	3.24	0.71	0.74	0.57	1.00	0.06	0.05	0.02
700_WH	0.60	0.93	0.72	5.76	8.93	5.56	0.71	0.76	0.62	0.98	0.12	0.26	0.03
400_PB	0.15	0.20	0.11	3.66	7.14	4.42	0.76	0.49	0.62	1.00	0.14	0.04	0.02
600_WB	0.10	0.08	0.09	3.80	6.82	5.56	0.91	0.56	0.32	0.99	0.19	0.01	0.01
Max	0.88	1.06	0.72	7.14	10.34	6.99	0.95	0.98	0.98	1.00	0.52	0.76	0.42
Min	0.1	0.08	0.09	3.01	6.31	3.16	0.52	0.49	0.32	0.21	0.05	0.01	0.01
Mean	0.39	0.59	0.39	4.55	8.10	4.78	0.70	0.80	0.76	0.92d	0.15	0.17	0.06
95% lower CI[b]	0.34	0.51	0.33	4.18	7.82	4.46	0.65	0.73	0.70	0.87	0.12	0.12	0.04
95% upper CI	0.48	0.69	0.44	4.95	8.39	5.22	0.75	0.83	0.81	0.97	0.19	0.23	0.09
SD[c]	0.18	0.26	0.16	1.05	0.84	0.83	0.15	0.13	0.16	0.15	0.10	0.17	0.08
CV[d] (%)	45	45	42	23	10	17	21	16	21	16	67	99	122

[a]The $RMSE_1$, $RMSE_2$, and $RMSE_3$ values refer to root-mean-squared error of modeling scenario 1, 2, and 3. For scenario 1, the generic model parameters were used, whereas biochar-specific Q_{max} values and generic log $\tilde{K}$ and m values were used in scenario 2. For scenario 3, all parameters are biochar-specific. The R^2 given here is for scenario 3. For the Donnan model, a fixed V_D of 0.1 L kg^{-1} was used in all three scenarios. [b]Confidence interval. [c]Standard deviation. [d]Coefficient of variation.

density of our 20 newly-produced biochars at pH 9 increased by 10% (from -3.50×10^4 to -3.84×10^4 C kg^{-1}) when the ionic strength increased from 0.01 to 0.1 M. For the same pH and ionic strength conditions, the charge densities simulated with generic NICA-Donnan model parameters[24] increased by 3% for FA (from -5.77×10^5 to -5.95×10^5 C kg^{-1}) and 5% for HA (from -3.86×10^5 to -4.04×10^5 C kg^{-1}). In contrast, the average charge density of our 20 newly-produced biochars at pH 4 increased by 4% (from 1.02×10^4 to 1.06×10^4 C kg^{-1}) when the ionic strength increased from 0.01 to 0.1 M, whereas the charge densities of FA and HA for the same conditions increased by 15% (from -2.68×10^5 to -3.09×10^5 C kg^{-1}) and 29% (from -1.12×10^5 to -1.44×10^5 C kg^{-1}), respectively.

3.3. Modeling Proton Binding to Individual Biochars.

The three-site NICA-Donnan model was fitted to the pH-charge density curves of all 36 biochars used in this study to derive the proton binding parameters for each individual biochar following the steps in SI-4. Fitting with a free-to-float V_D parameter was unsuccessful because the iteration process in the FIT program did not converge into a solution for V_D. This is probably because the three-site NICA-Donnan model has

https://doi.org/10.1021/acssusresmgt.3c00104
ACS Sustainable Resour. Manage. 2024, 1, 707−720

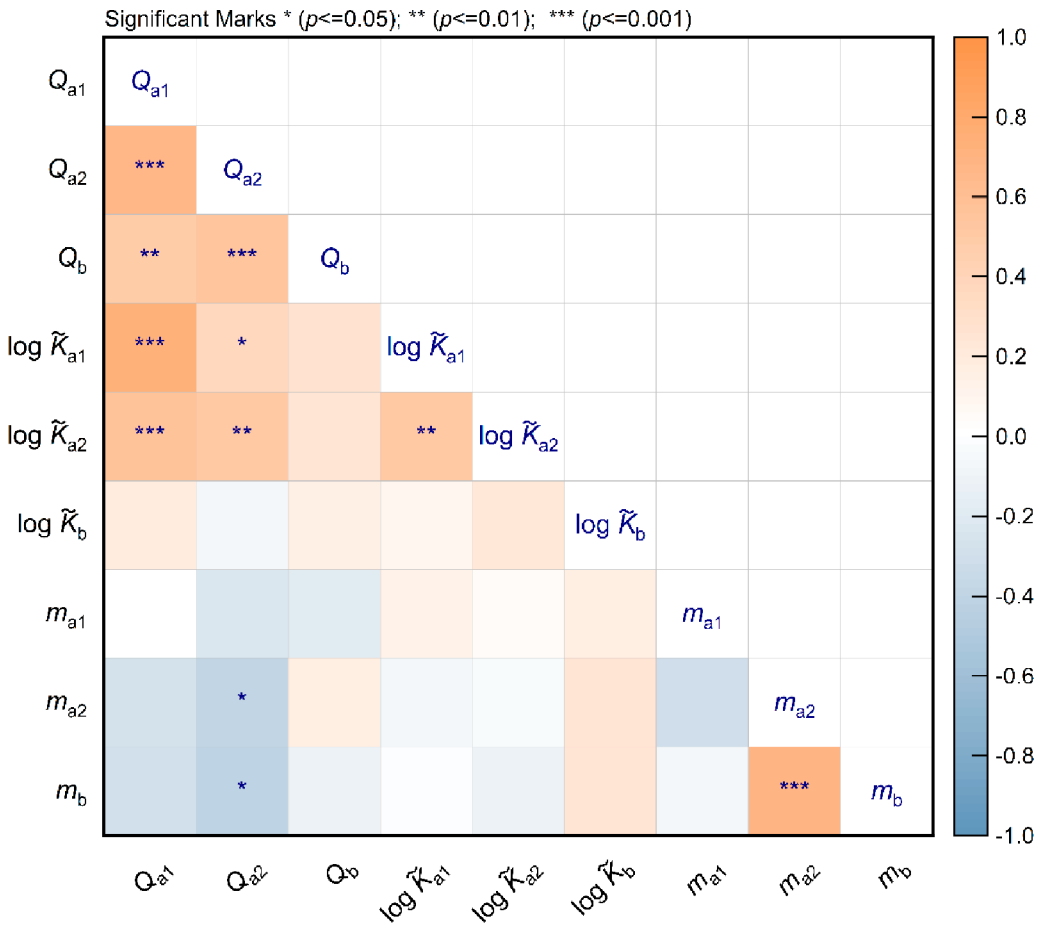

Figure 4. Correlations between the three-site NICA-Donnan parameters based on the results of biochar-specific model parameters of the 36 biochars studied in the current work (Table 1). The correlation coefficients are indicated by the color scale. The level of significance was expressed using * for $p < 0.05$, ** for $p < 0.01$, and *** for $p < 0.001$.

three extra parameters for the basic group requiring fitting as compared to the classical two-site model. Alternatively, we used a constant V_D for all biochars in the Donnan model. The V_D was derived by step-wise increasing the volume from 0.01 to 1 L kg^{-1}, while testing R^2 and the root-mean-squared error (RMSE) of the experimental versus modelled data (see SI-5). In the end, a V_D of 0.1 L kg^{-1} was chosen because the average R^2 increased whereas the RMSE decreased when increasing V_D from 0.01 to 0.1 L kg^{-1} (Figure S2). Increasing V_D from 0.1 to 1 L kg^{-1} did not further increase the R^2 and decrease the RMSE. The V_D of 0.1 L kg^{-1} is higher than the average pore volume of 0.04 L kg^{-1} of wood-, chicken manure-, and water hyacinth-based biochars pyrolyzed at a temperature of 300°C but lower than the pore volume of 0.15 L kg^{-1} for biochars of the same materials pyrolyzed at 600°C.[49] Since the biochar pore volume increases with pyrolysis temperature,[66] the fitted generic V_D of 0.1 L kg^{-1} for all 36 biochars used in our work should be interpreted as an average pore volume, as they were produced at temperatures between 60−700°C (Table S1).

The pH-charge density curves of the 36 biochars could be well described with the three-site NICA-Donnan model using biochar-specific parameters with an R^2 = 0.82−1.00, except for two biochars with an R^2 = 0.21 and 0.57 (Table 1). The site density Q_{max} for the 36 biochars varies between 0.1−0.88, 0.08−1.06, and 0.09−0.72 mol kg^{-1} for the carboxylic-type (site$_{a1}$), phenolic-type (site$_{a2}$), and basic (site$_b$) groups, respectively. The median proton affinity constant log $\tilde{K}$ of the two acidic groups is between 3.01−7.14 (log $\tilde{K}_{a1}$) and 6.31−10.34 (log $\tilde{K}_{a2}$), whereas log $\tilde{K}_b$ varies between 3.16−6.99. The heterogeneity parameter (m) is between 0.52−0.95 (m_{a1}), 0.49−0.98 (m_{a2}), and 0.32−0.98 (m_b).

Compared to the generic NICA-Donnan parameters for FA and HA, the biochars have on average less carboxylic- ($Q_{max,a1}$ = 0.39 mol kg^{-1}) and phenolic-type groups ($Q_{max,a2}$ = 0.59 mol kg^{-1}) (Table 1) than FA ($Q_{max,a1}$ = 5.88 mol kg^{-1}, $Q_{max,a1}$ = 1.86 mol kg^{-1}) and HA ($Q_{max,a1}$ = 3.15 mol kg^{-1}, $Q_{max,a2}$ = 2.55 mol kg^{-1}).[24] Hence, the average total content of reactive acidic groups (*i.e.*, $Q_{max,a1}$ + $Q_{max,a2}$) of biochar is ∼8 and ∼6 times lower than the total content of FA and HA, respectively. Since the biochar structure is more aromatized and ordered compared to humic substances, fewer carbon atoms are present in surface functional groups.[67] For humic substances, the site density of carboxylic-type groups is higher than for the phenolic-type groups.[24] For biochar, however, the opposite was found as phenolic-type groups have the highest density among the three reactive groups, consistent with their more aromatic character. Furthermore, the affinity of carboxylic-type groups of biochar for proton binding is higher (log $\tilde{K}_{a1}$ = 4.55) than the affinity of the same type of groups of both FA (log $\tilde{K}_{a1}$ = 2.34) and HA (log $\tilde{K}_{a1}$ = 2.93). Hence, carboxylic-type groups in biochar are less acidic. In contrast, the log $\tilde{K}_{a2}$ of the phenolic-type groups of biochar (8.10) agrees reasonably well with the log $\tilde{K}_{a2}$ of FA (8.60), whereas it is close to the log $\tilde{K}_{a2}$ of HA (8.00).[24] In the NICA model concept,[19] each type of

https://doi.org/10.1021/acssusresmgt.3c00104
ACS Sustainable Resour. Manage. 2024, 1, 707−720

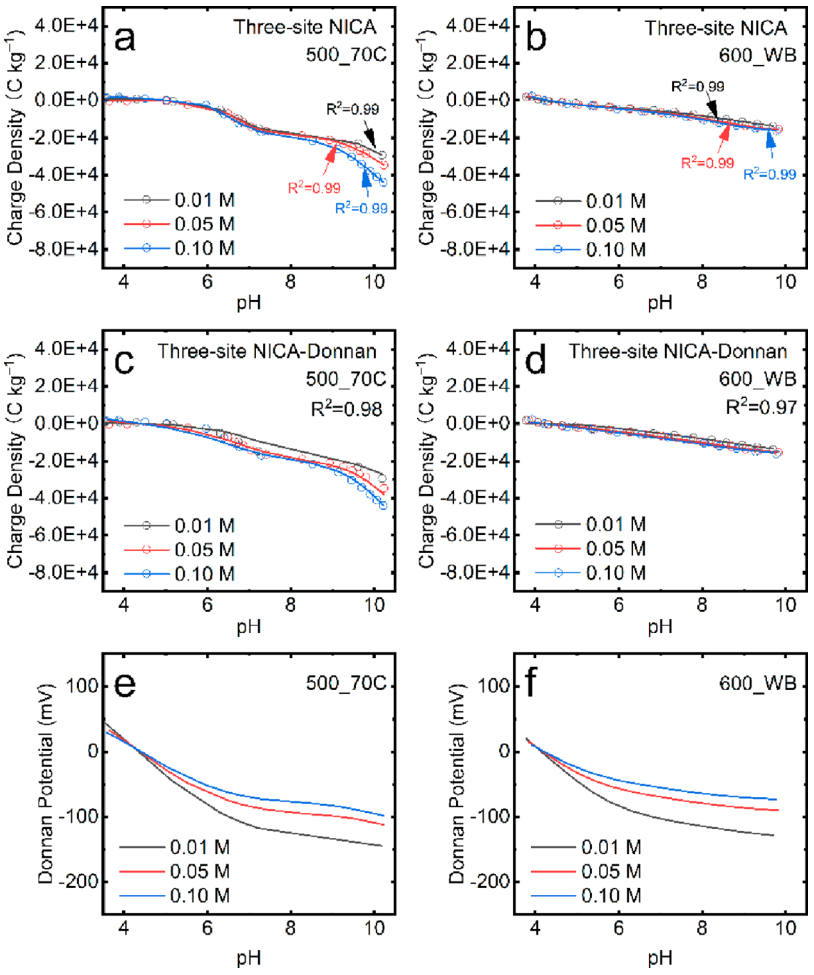

Figure 5. pH-charge density curves of two biochars (*i.e.*, 500_70C and 600_WB) at different ionic strength (0.01, 0.05, and 0.1 M NaCl) measured and modelled with three-site NICA (a and b) and three-site NICA-Donnan model (c and d) and the Donnan potential calculated (e and f).

reactive group contains a range of similar groups, which are influenced by their nearby molecular structures. This will, in turn, lead to heterogeneity in the binding affinity toward protons as described by the heterogeneity parameter m. Since m is higher and closer to 1 for both the carboxylic- and phenolic-type groups of biochar (m_{a1} = 0.70, m_{a2} = 0.80) compared to FA (m_{a1} = 0.38, m_{a2} = 0.53) and HA (m_{a1} = 0.50, m_{a2} = 0.26), there is less heterogeneity in proton binding affinity by carboxylic- and phenolic-type groups of biochar than for humic substances. This can be explained by the concentration of carbon as aromatic carbon and the emergence of a highly-ordered graphite-like structure during biomass pyrolysis,[68−70] translating into a less variable chemical structure of biochars. The heterogeneity parameter m of the three reactive groups in the three-site NICA-Donnan model for the 36 biochars decreases in the order of $m_{a2} > m_b > m_{a1}$. Hence, the heterogeneity in proton binding affinity by the three reactive groups follows the order of site$_{a1}$> site$_b$ > site$_{a2}$.

The NICA model parameters were further analyzed by exploring how they relate to pyrolysis temperature (Figure S3). The $Q_{max,a1}$ decreases linearly with pyrolysis temperature (p < 0.01) whereas m_{a1} increases linearly with temperature (p < 0.05), consistent with the observed formation of a highly-ordered aromatic carbon structure with the increase of temperature.[68,69] For the other NICA model parameters, no significant relationships with pyrolysis temperature were observed. The decrease in the site density of the carboxylic-type groups with pyrolysis temperature explains why the PZC of biochars washed either with HCl or NaOH/HCl increases with temperature (Figure 3). Furthermore, we have performed a correlation analysis of the NICA model parameters fitted for our 36 biochars (Figure 4). There is a significant positive correlation (p < 0.01) among the site densities (Q_{max}) of all the three types of sites. Likewise, there is a significant positive correlation between the protonation constants (log $\tilde{K}$) of the two acidic groups and their site densities (Q_{max}) (p < 0.01). The proton affinity constant of the basic group (log $\tilde{K}_b$) is not significantly correlated with any of the model parameters. However, the heterogeneity parameter of the basic group (m_b) is significantly positively correlated with the heterogeneity parameter of the phenolic-type groups (m_{a2}) (p < 0.001), and both m_b and m_{a2} are significantly negatively correlated with the site density of the phenolic-type groups (p < 0.05). The model parameters of the basic group are even better correlated with those of the phenolic-type groups than with those of the carboxylic-type groups. This further indicates the necessity to include the basic group in the NICA model. However, the correlations between the model parameters make it even more complicated to simultaneously fit the NICA model parameters for all 36 biochars, as is discussed further in Section 3.4. Therefore, we have derived our generic parameters using the average values of all biochars.

https://doi.org/10.1021/acssusresmgt.3c00104
ACS Sustainable Resour. Manage. 2024, 1, 707−720

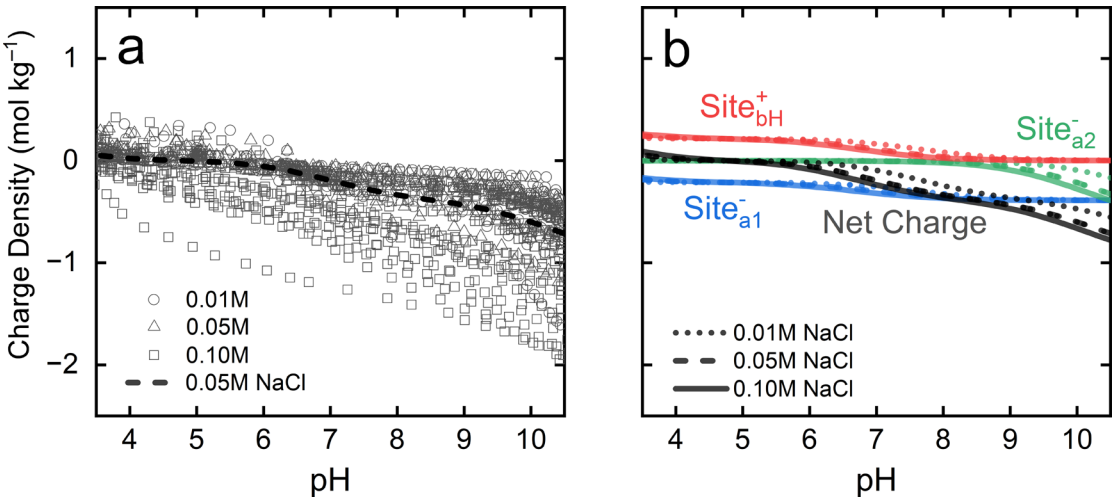

Figure 6. Figure 6a: An overview of the experimental pH-charge density curves of the 36 biochars, including the 20 biochars produced in this study and the 16 other biochars from Li et al.[39] and Xiong et al.[21] at an ionic strength of 0.01, 0.05, and 0.1 M NaCl. The dashed line represents the curve calculated at an ionic strength of 0.05 M NaCl using the three-site NICA-Donnan model with generic proton binding parameters (Table 1). Figure 6b: pH-charge density curves of the two acidic-type groups and the basic group as well as the net charge of an "average" biochar calculated using our generic three-site NICA-Donnan model parameters at three different ionic strengths. $Site_{a1}$ represents carboxylic-type groups, $site_{a2}$ represents phenolic-type groups, and $site_b$ represents basic groups.

For the three-site NICA model used by Xiong et al.,[21] the average log $\tilde{K}_{a1}$, log $\tilde{K}_{a2}$, and log $\tilde{K}_b$ values of their two biochars changed from 3.49 to 3.60, 9.42 to 8.41, and 6.84 to 5.98, respectively, when the ionic strength increased from 0.01 to 0.1 M. The pH-charge density curves of two biochars, *i.e.*, 500_70C (prepared in our study) and 600_WB (originally named TWB in Xiong et al.[21]) measured at three ionic strengths are described in Figure 5, using either the three-site NICA model with the biochar-specific but ionic strength-dependent log $\tilde{K}$ and m parameters or the three-site NICA-Donnan model with one set of biochar-specific proton binding parameters as derived here (Table 1). For our 500_70C biochar, we fitted the conditional log $\tilde{K}$ and m parameters ourselves, whereas we used the conditional log $\tilde{K}$ and m parameters for the 600_WB biochar from Xiong et al.[21] Clearly, the pH-charge density curves can be modelled just as well with our single set of intrinsic three-site NICA-Donnan parameters as with the ionic-strength-dependent parameters.

The log $\tilde{K}_{a1}$ values derived for the 500_70C and 600_WB biochars using our three-site NICA-Donnan model (Table 1) are higher than the ionic strength-dependent log $\tilde{K}_{a1}$ values of the three-site NICA model from Xiong et al.[21] (ionic strength range = 0.01−0.1 M; 500_70C: log $\tilde{K}_{a1}$ = 4.03−4.36; 600_WB: log $\tilde{K}_{a1}$ = 3.45−3.58), whereas the log $\tilde{K}_{a2}$ and log $\tilde{K}_b$ values derived for these biochars with our model (Table 1) are lower than those of the three-site NICA model (ionic strength range = 0.01−0.1 M; 500_70C: log $\tilde{K}_{a2}$ = 10.77−10.38, log $\tilde{K}_b$ = 6.85−6.7; 600_WB: log $\tilde{K}_{a2}$ = 9.12−8.33, log $\tilde{K}_b$ = 6.96−6.35). Since Ψ_D decreased from being positive when the pH is <PZC to negative when the pH is >PZC (Figure 5), $[H_D]$ changes from being lower than (H_{aq}) to higher than (H_{aq}). For example, Ψ_D varied from 10 to −130 mV for the 600_WB biochar when the pH increased from 3.5 to 10.5 at an ionic strength of 0.01 M. Since the log $\tilde{K}_{a1}$ values of the 500_70C and 600_WB biochars are below the PZC, they have a positive charge and Ψ_D. Consequently, $[H_D]$ is lower than (H_{aq}), explaining why the intrinsic log $\tilde{K}_{a1}$ values of our three-site NICA-Donnan model are higher than the conditional log $\tilde{K}_{a1}$ values of Xiong et al.[21] Since the log $\tilde{K}_{a2}$ and log $\tilde{K}_b$ values of both biochars are above the PZC where they have a negative charge and Ψ_D, $[H_D]$ is higher than (H_{aq}). Consequently, the intrinsic log $\tilde{K}_{a2}$ and log $\tilde{K}_b$ values of our three-site NICA-Donnan model are lower.

3.4. Generic Three-Site NICA-Donnan Model Parameters. For predicting the "average" charging behavior of a biochar when specific NICA-Donnan parameters for a particular biochar are unavailable, generic parameters are needed. Generic NICA-Donnan model parameters have been derived for FA and HA by Milne et al.[24] We attempted to derive the generic three-site NICA-Donnan model parameters for biochar in a simultaneous fit of the pH-charge density curves of all 36 biochars. In our approach, each curve contributed equally to the overall dataset, while the nine parameters (Q_{max}, log $\tilde{K}$ and m for three types of sites) of the NICA model were optimized simultaneously and V_D was fixed at 0.1 L kg^{-1}. However, this approach, as Milne et al.[24] experienced as well, was unsuccessful, which in both cases was probably due to the large number of parameters requiring simultaneous optimization[71] and parameters not being independent of each other (Figure 4).[31,71,72] Our model considers three types of sites rather than the two as in the work of Milne et al.[24] Hence, simultaneous fitting of all parameters is even more challenging in our case. Milne et al.[24] solved this problem by deriving the generic log $\tilde{K}$ and m in a first fitting step and the generic Q_{max} in a second one, using an adapted version of the FIT program[56] with a maximum capacity of 16 datasets. Milne et al.[24] limited the number of FA and HA datasets to 11 and 15, respectively, by excluding datasets with either a short pH range or for which the fit quality of the individual proton binding parameters was low. Since the pH range used in the acid−base titration experiments was broad for all 36 biochars (Table S1) and because the proton binding behavior of nearly all individual biochars could be well described by our biochar-specific parameters, we took the means of the biochar-specific parameters as generic values (Table 1). This approach is reasonable because the mean values of most NICA model parameters for individual FA and HA were close to their generic values derived by Milne et al.[24]

https://doi.org/10.1021/acssusresmgt.3c00104
ACS Sustainable Resour. Manage. 2024, 1, 707−720

(<4% difference). In Figure 6, we compared the pH-charge density curve of an "average" biochar at an ionic strength of 0.05 M NaCl as calculated using our set of recommended generic proton binding parameters to the experimental curves of all 36 biochars.

On the basis of our set of generic parameters, the charge of each of the three types of reactive groups considered in the NICA-Donnan model was calculated as a function of pH and ionic strength (Figure 6). Each site can exist in a protonated and deprotonated form: $site^{0}_{a1H}$, $site^{-}_{a1H}$, $site^{0}_{a2H}$, $site^{-}_{a2}$, $site^{+}_{bH}$, and $site^{0}_{b}$. Hence, the net charge of these sites equals the sum of $(site^{-}_{a1})$ + $(site^{-}_{a2})$ + $(site^{+}_{bH})$. From a low pH (e.g., pH 3) to a pH of ∼5, $site_b$ becomes less positively charged whereas $site_{a1}$ becomes more negatively charged. Since the site density as well as the log $\tilde{K}$ values of the carboxylic- and basic-type groups are close to each other (Table 1), the negative and positive charge of these reactive groups compensate each other when the pH equals their log $\tilde{K}$, with the net charge of the biochar becoming zero, *i.e.*, the PZC. When the pH is >PZC, the positive charge of the basic group can no longer fully compensate the negative charge of the carboxylic-type groups and the net charge becomes negative. When the pH is >7, the phenolic-type groups start to deprotonate, resulting in an even more net negative charge of the biochar. For the charging curve of each individual group, the log $\tilde{K}$ corresponds to the midpoint of the S-shaped curve, Q_{max} determines the maximum charge, and m determines the smoothness of the curve. When m becomes smaller, the binding site heterogeneity increases, leading to a smoother curve. The ionic strength influences the charge of each group the most at a pH close to their log $\tilde{K}$ because at this pH protonation of binding sites and the resulting charge are most sensitive to a change in the local proton concentration in the Donnan phase $[H_D]$. The $[H_D]$ is influenced by the Donnan potential Ψ_D, which changes with ionic strength at a given pH. At a pH further away from the log $\tilde{K}$, the sites are either almost fully protonated (low pH) or deprotonated (high pH). Therefore, a change in the ionic strength will influence the charge and protonation of a specific group to a lesser extent than at a pH close to its log $\tilde{K}$.

To enable the reader to make a well-considered choice to either use a set of generic NICA-Donnan parameters or to experimentally derive some or all of the parameters when modeling proton binding to a specific plant-based biochar, we compared the performance of our generic parameters for describing proton binding to all 36 biochars (scenario 1) against two alternative scenarios in which either a combination of biochar-specific and generic parameters (scenario 2) or only biochar-specific parameters (scenario 3) were used. For scenario 2, we used biochar-specific Q_{max} values for each of the three reactive groups in combination with generic log $\tilde{K}$ and m values. We have chosen to use biochar-specific Q_{max} values in this scenario as Q_{max} shows the largest degree of variation among the proton binding parameters, with a coefficient of variation (CV) of 42−45% (Table 1). The CV of log $\tilde{K}$ follows the order of log $\tilde{K}_{a1}$ (23%) > log $\tilde{K}_{b}$ (17%) > log $\tilde{K}_{a2}$ (10%). For the heterogeneity parameter m, the CV is 21% (m_{a1}), 16% (m_{a2}), and 21% (m_b). For the three scenarios, we calculated the RMSE of the experimental versus modelled data for all individual biochars (Table 1). Obviously, using biochar-specific parameters (scenario 3) gives the best fit, with an average RMSE of 0.06 ± 0.08 mol kg^{-1}. When experimental acid−base titration data are available, deriving biochar-specific three-site NICA-Donnan model parameters will lead to the best possible description of the charging behavior for the biochar of interest. The average RMSE of scenario 1 is 0.15 ± 0.10 mol kg^{-1} when all three-site NICA model parameters are generic. The use of a biochar-specific Q_{max} in combination with generic log $\tilde{K}$ and m (scenario 2) leads to an average RMSE of 0.17 ± 0.17 mol kg^{-1}. Hence, the goodness-of-fit of scenario 1 with only generic parameters is even slightly better than the fit quality of scenario 2 when biochar-specific Q_{max} values are used. When titration data of a particular plant-based biochar are unavailable, one can thus generate its pH-charge density curve best by using the full set of recommended generic three-site NICA-Donnan model parameters as derived in this study (Table 1). Scaling the RMSE of scenario 1 using only generic parameters against the absolute range in proton adsorption across all 36 biochars yields a relative error of ∼6%. For humic substances, the same approach gives an error of 10% (FA) and 11% (HA).[24] Hence, the generic proton binding parameters for biochars recommended here (Table 1) have an even better predictive capability than the generic parameters derived by Milne et al.[24] for FA and HA, while they have extensively demonstrated their value in modelling proton binding to humic substances as a prerequisite for modelling proton buffering and pH-control[73] and the bioavailability and mobility of trace metals in natural soils and aquatic systems.[26−33]

3.5. Environmental Implications. The set of generic proton binding parameters of the three-site NICA-Donnan model derived for the plant-based biochars in this study lays the basis for further model parameterization that includes binding parameters for trace metals. This will facilitate application of the three-site NICA-Donnan model to assess the capacity and affinity of biochars to bind trace metals like Cd, Cu, Ni, Pb, and Zn over a wide range in soil properties including pH, ionic strength, and the presence of other competing/synergistic ions. Embedding the three-site NICA-Donnan model in a so-called process-based multi-surface modelling (MSM) approach[74] subsequently enables evaluation of the solid-solution partitioning and speciation of trace metals in polluted soils amended with biochar as a potential remediation strategy. In the MSM approach, separate SCMs are combined for each of the reactive components present in soils, including organic matter, clay minerals, and Fe- and Al-oxides, while embedding the three-site NICA-Donnan model would add biochar as an additional reactive surface and extend the applicability of this approach to biochar-amended soils. Since mechanistic SCMs are independent of environmental conditions (*e.g.*, pH and ionic strength),[74] the MSM approach including the three-site NICA-Donnan model is applicable to soils with a wide range in soil properties.[75,76] Additionally, SCMs account for the presence of competitive ions,[74] which is of pivotal importance as multiple trace metals are often simultaneously present at elevated levels in polluted soils.[76,77] An essential next step toward this goal is to collect experimental data on the binding of various trace metals by plant-based biochars to derive trace metal binding parameters for the three-site NICA-Donnan model, analogous to the approach taken for the classical two-site NICA model for FA and HA.[25] Likewise, derivation of binding parameters for oxyanionic pollutants like arsenite (AsO_3^{3-}) and arsenate (AsO_4^{3-}) is important, as these anions can also bind to biochar, especially in case of a pH <PZC when the net surface charge is positive.[78] This perspective of a MSM extended with the three-site NICA-Donnan model and binding parameters for protons, metals, and oxyanions as outlined above is also

https://doi.org/10.1021/acssusresmgt.3c00104
ACS Sustainable Resour. Manage. 2024, 1, 707−720

highly relevant for the potential use of biochar as a soil amendment in the context of improving important soil functions such as water and nutrient retention in support of soil fertility and agricultural production.[10] In this context, trace metals like Cu and Zn are essential micronutrients for crop growth[79] but can become toxic when present in excess. The application of biochar to agricultural soils with low levels of micronutrients like Cu and Zn can potentially lead to a reduction in the bioavailability of these essential micronutrients for uptake by arable crops.[80,81] The same can happen with macronutrients such as nitrogen in the form of NH_4^+, K, and phosphate, as they can bind to biochar as well.[82−84] Application of biochar thus requires careful tailoring to the targeted soil function and specific soil properties, which can be strongly facilitated by the outlined further parameterization and implementation of the three-site NICA-Donnan model in MSM frameworks. This perspective then also extends to evaluation of potential beneficial and/or adverse side effects of biochar application for the purpose of soil carbon sequestration.

3.6. Conclusions. In this study, the pH-charge curves of 20 newly-produced biochars were measured, whereas curves of 16 other biochars were collected from literature. All 36 biochars were produced from different plant-based materials at various pyrolysis temperatures. The pH-charging data were used to derive proton binding parameters for a novel three-site NICA-Donnan model, accounting for proton binding to carboxylic ($site_{a1}$) and phenolic ($site_{a2}$) acidic groups as well as to a basic ($site_b$) group. The key findings are as follows: (i) The pH-charge density curves of the 20 newly-produced biochars measured at the three ionic strengths of 0.01, 0.05, and 0.1 M revealed a PZC between pH 4.8−6.6, which can be explained by the presence of both acidic and basic groups. When the pH is <PZC, the biochars have a net weak positive charge, whereas they have a net negative charge when the pH is >PZC. (ii) The model successfully described the proton binding behavior of the 36 biochars at different ionic strengths for the first time, by extending the classical two-site NICA model with a basic group in combination with an electrostatic Donnan model using a fixed volume of 0.1 L kg^{-1}. (iii) A suite of spectroscopic techniques including NMR, XPS, and FTIR was used to validate the presence of the three types of reactive groups considered in the model. The results of the spectroscopic characterization of selected biochars confirmed the presence of carboxylic and phenolic groups and basic groups like N-containing heterocyclic structures (*i.e.*, pyridine and graphitic-N). (iv) The proton binding parameters of the 36 biochars were used to derive a set of generic parameters, which can be used for modeling when specific parameters for a particular biochar are unavailable. Application of the recommended generic parameters resulted in a relative error of ∼6% for proton adsorption by all 36 biochars. (v) The set of generic proton binding parameters of the three-site NICA-Donnan model derived for the plant-based biochars in our study lays the basis for further model development including a quantitative description of trace metal adsorption.

■ ASSOCIATED CONTENT

Supporting Information

The Supporting Information is available free of charge at https://pubs.acs.org/doi/10.1021/acssusresmgt.3c00104.

Additional details for (i) acid−base titrations, (ii) spectroscopic techniques, (iii) literature review protocol on PZC and washing methods of biochars and statistics, and (iv) derivation of three-site NICA model parameters and Donnan volume; additional tables with (i) details for biochar preparation, (ii) results literature review, and (iii) ^{13}C NMR results for selected biochars; and additional figures with (i) PZC and washing methods of biochars, (ii) fitting results for the Donnan volume, and (iii) relationships between three-site NICA-Donnan model parameters and pyrolysis temperature (PDF)

■ AUTHOR INFORMATION

Corresponding Author

Liping Weng − *Chair group Soil Chemistry and Chemical Soil Quality, Wageningen University, Wageningen 6708 PB, The Netherlands; Agro-Environmental Protection Institute, Ministry of Agriculture and Rural Affairs, Tianjin 300191, China;* orcid.org/0009-0006-8045-0141; Email: liping.weng@wur.nl

Authors

Yifan Huang − *Chair group Soil Chemistry and Chemical Soil Quality, Wageningen University, Wageningen 6708 PB, The Netherlands; Agro-Environmental Protection Institute, Ministry of Agriculture and Rural Affairs, Tianjin 300191, China; Department of Civil and Environmental Engineering, Shantou University, Shantou 515063, China;* orcid.org/0000-0001-5578-5368

Gerwin F. Koopmans − *Chair group Soil Chemistry and Chemical Soil Quality, Wageningen University, Wageningen 6708 PB, The Netherlands;* orcid.org/0000-0002-3664-6650

Jan E. Groenenberg − *Chair group Soil Chemistry and Chemical Soil Quality, Wageningen University, Wageningen 6708 PB, The Netherlands;* orcid.org/0000-0002-3227-4052

Zhengguo Song − *Department of Civil and Environmental Engineering, Shantou University, Shantou 515063, China;* orcid.org/0000-0003-4393-0622

Rob N. J. Comans − *Chair group Soil Chemistry and Chemical Soil Quality, Wageningen University, Wageningen 6708 PB, The Netherlands*

Complete contact information is available at: https://pubs.acs.org/10.1021/acssusresmgt.3c00104

Author Contributions

All authors have contributed to the writing of this manuscript and given approval to the final version.

Notes

The authors declare no competing financial interest.

■ ACKNOWLEDGMENTS

This study was funded by the National Natural Science Foundation of China (no. 41771525), STU Scientific Research Foundation for Talents (NTF19025). Y.H. was sponsored by the China Scholarship Council (202003250108). The authors would like to thank the editor and anonymous reviewers for their insightful comments and suggestions, which helped improve this work.

REFERENCES

(1) Weber, K.; Quicker, P. Properties of Biochar. *Fuel* **2018**, *217*, 240−261.

(2) Ahmad, M.; Rajapaksha, A. U.; Lim, J. E.; Zhang, M.; Bolan, N.; Mohan, D.; Vithanage, M.; Lee, S. S.; Ok, Y. S. Biochar as a Sorbent for Contaminant Management in Soil and Water: a Review. *Chemosphere* **2014**, *99*, 19−33.

(3) Mahar, A.; Wang, P.; Li, R.; Zhang, Z. Immobilization of Lead and Cadmium in Contaminated Soil Using Amendments: A Review. *Pedosphere* **2015**, *25* (4), 555−568.

(4) El-Naggar, A.; Chang, S. X.; Cai, Y.; Lee, Y. H.; Wang, J.; Wang, S.-L.; Ryu, C.; Rinklebe, J.; Sik Ok, Y. Mechanistic Insights into the (Im)mobilization of Arsenic, Cadmium, Lead, and Zinc in a Multi-Contaminated Soil Treated with Different Biochars. *Environ. Int.* **2021**, *156*, 106638.

(5) O'Connor, D.; Peng, T.; Li, G.; Wang, S.; Duan, L.; Mulder, J.; Cornelissen, G.; Cheng, Z.; Yang, S.; Hou, D. Sulfur-Modified Rice Husk Biochar: A Green Method for The Remediation of Mercury Contaminated Soil. *Science of The Total Environment* **2018**, *621*, 819−826.

(6) Kazemi Shariat Panahi, H.; Dehhaghi, M.; Ok, Y. S.; Nizami, A.-S.; Khoshnevisan, B.; Mussatto, S. I.; Aghbashlo, M.; Tabatabaei, M.; Lam, S. S. A Comprehensive Review of Engineered Biochar: Production, Characteristics, and Environmental Applications. *Journal of Cleaner Production* **2020**, *270*, 122462.

(7) Khosravi, A.; Zheng, H.; Liu, Q.; Hashemi, M.; Tang, Y.; Xing, B. Production and Characterization of Hydrochars and Their Application in Soil Improvement and Environmental Remediation. *Chemical Engineering Journal* **2022**, *430*, 133142−133142.

(8) Liu, W. J.; Jiang, H.; Yu, H. Q. Development of Biochar-Based Functional Materials: Toward a Sustainable Platform Carbon Material. *Chem. Rev.* **2015**, *115* (22), 12251−12285.

(9) Xiang, L.; Harindintwali, J. D.; Wang, F.; Redmile-Gordon, M.; Chang, S. X.; Fu, Y.; He, C.; Muhoza, B.; Brahushi, F.; Bolan, N.; et al. Integrating Biochar, Bacteria, and Plants for Sustainable Remediation of Soils Contaminated with Organic Pollutants. *Environ. Sci. Technol.* **2022**, *56* (23), 16546−16566.

(10) Singh Yadav, S. P.; Bhandari, S.; Bhatta, D.; Poudel, A.; Bhattarai, S.; Yadav, P.; Ghimire, N.; Paudel, P.; Paudel, P.; Shrestha, J.; Oli, B. Biochar Application: A Sustainable Approach to Improve Soil Health. *Journal of Agriculture and Food Research* **2023**, *11*, 100498.

(11) Ok, Y. S.; Bhatnagar, A.; Hou, D.; Bhaskar, T.; Masek, O. Advances in Algal Biochar: Production, Characterization and Applications. *Bioresource Technology* **2020**, *317*, 123982.

(12) Ippolito, J. A.; Cui, L.; Kammann, C.; Wrage-Mönnig, N.; Estavillo, J. M.; Fuertes-Mendizabal, T.; Cayuela, M. L.; Sigua, G.; Novak, J.; Spokas, K.; Borchard, N. Feedstock Choice, Pyrolysis Temperature and Type Influence Biochar Characteristics: A Comprehensive Meta-Data Analysis Review. *Biochar* **2020**, *2* (4), 421−438.

(13) Vassilev, S. V.; Baxter, D.; Andersen, L. K.; Vassileva, C. G.; Morgan, T. J. An Overview of the Organic and Inorganic Phase Composition of Biomass. *Fuel* **2012**, *94* (1), 1−33.

(14) UC Davis Biochar Database. https://biochar.ucdavis.edu/ (accessed 2021-09-01).

(15) Wan, J.; Liu, L.; Ayub, K. S.; Zhang, W.; Shen, G.; Hu, S.; Qian, X. Characterization and Adsorption Performance of Biochars Derived from Three Key Biomass Constituents. *Fuel* **2020**, *269*, 117142−117142.

(16) Tessier, A.; Campbell, P. G.; Bisson, M. Sequential Extraction Procedure for the Speciation of Particulate Trace Metals. *Analytical Chemistry* **1979**, *51* (7), 844−851.

(17) Weng, L.; Temminghoff, E. J.; Lofts, S.; Tipping, E.; Van Riemsdijk, W. H. Complexation with Dissolved Organic Matter and Solubility Control of Heavy Metals in a Sandy Soil. *Environ. Sci. Technol.* **2002**, *36* (22), 4804−4810.

(18) Van Eynde, E.; Groenenberg, J. E.; Hoffland, E.; Comans, R. N. J. Solid-Solution Partitioning of Micronutrients Zn, Cu and B in Tropical Soils: Mechanistic and Empirical Models. *Geoderma* **2022**, *414*, 115773.

(19) Benedetti, M. F.; Milne, C. J.; Kinniburgh, D. G.; Van Riemsdijk, W. H.; Koopal, L. K. Metal Ion Binding to Humic Substances: Application of the Non-Ideal Competitive Adsorption Model. *Environ. Sci. Technol.* **1995**, *29* (2), 446−457.

(20) Hiemstra, T.; De Wit, J. C. M.; Van Riemsdijk, W. H. Multisite Proton Adsorption Modeling at the Solid/Solution Interface of (Hydr)Oxides: A New Approach. *J. Colloid Interface Sci.* **1989**, *133* (1), 105−117.

(21) Xiong, J.; Xu, J.; Zhou, M.; Zhao, W.; Chen, C.; Wang, M.; Tan, W.; Koopal, L. Quantitative Characterization of the Site Density and the Charged State of Functional Groups on Biochar. *ACS Sustainable Chem. Eng.* **2021**, *9* (6), 2600−2608.

(22) Kinniburgh, D. G.; Milne, C. J.; Benedetti, M. F.; Pinheiro, J. P.; Filius, J.; Koopal, L. K.; Van Riemsdijk, W. H. Metal Ion Binding by Humic Acid: Application of the NICA-Donnan Model. *Environ. Sci. Technol.* **1996**, *30* (5), 1687−1698.

(23) Koopal, L. K.; Saito, T.; Pinheiro, J. P.; Van Riemsdijk, W. H. Ion Binding to Natural Organic Matter: General Considerations and the NICA-Donnan Model. *Colloids Surf., A* **2005**, *265* (1-3), 40−54.

(24) Milne, C. J.; Kinniburgh, D. G.; Tipping, E. Generic NICA-Donnan Model Parameters for Proton Binding by Humic Substances. *Environ. Sci. Technol.* **2001**, *35* (10), 2049−2059.

(25) Milne, C. J.; Kinniburgh, D. G.; van Riemsdijk, W. H.; Tipping, E. Generic NICA-Donnan Model Parameters for Metal-Ion Binding by Humic Substances. *Environ. Sci. Technol.* **2003**, *37* (5), 958−971.

(26) Koopmans, G. F.; Schenkeveld, W. D.; Song, J.; Luo, Y.; Japenga, J.; Temminghoff, E. J. Influence of EDDS on Metal Speciation in Soil Extracts: Measurement and Mechanistic Multi-component Modeling. *Environ. Sci. Technol.* **2008**, *42* (4), 1123−1130.

(27) Tan, W.; Xiong, J.; Li, Y.; Wang, M.; Weng, L.; Koopal, L. K. Proton Binding to Soil Humic and Fulvic Acids: Experiments and NICA-Donnan Modeling. *Colloids Surf., A* **2013**, *436*, 1152−1158.

(28) Van Eynde, E.; Weng, L.; Comans, R. N. J. Boron Speciation and Extractability in Temperate and Tropical Soils: A Multi-Surface Modeling Approach. *Applied Geochemistry* **2020**, *123*, 104797−104797.

(29) Xiong, J.; Koopal, L. K.; Weng, L.; Wang, M.; Tan, W. Effect of Soil Fulvic and Humic Acid on Binding of Pb to Goethite-Water Interface: Linear Additivity and Volume Fractions of HS in the Stern Layer. *J. Colloid Interface Sci.* **2015**, *457*, 121−130.

(30) Unsworth, E. R.; Warnken, K. W.; Zhang, H.; Davison, W.; Black, F.; Buffle, J.; Cao, J.; Cleven, R.; Galceran, J.; Gunkel, P.; et al. Model Predictions of Metal Speciation in Freshwaters Compared to Measurements by In Situ Techniques. *Environ. Sci. Technol.* **2006**, *40* (6), 1942−1949.

(31) Groenenberg, J. E.; Koopmans, G. F.; Comans, R. N. Uncertainty Analysis of the Nonideal Competitive Adsorption-Donnan Model: Effects of Dissolved Organic Matter Variability on Predicted Metal Speciation in Soil Solution. *Environ. Sci. Technol.* **2010**, *44* (4), 1340−1346.

(32) Avendaño, L.; Gledhill, M.; Achterberg, E. P.; Rérolle, V. M. C.; Schlosser, C. Influence of Ocean Acidification on the Organic Complexation of Iron and Copper in Northwest European Shelf Seas; A Combined Observational and Model Study. *Frontiers in Marine Science* **2016**, *3*, 1 DOI: 10.3389/fmars.2016.00058.

(33) Hiemstra, T.; van Riemsdijk, W. H. Biogeochemical Speciation of Fe in Ocean Water. *Marine Chemistry* **2006**, *102* (3-4), 181−197.

(34) Pereira, R. C.; Arbestain, M. C.; Sueiro, M. V.; Maciá-Agulló, J. A. Assessment of the Surface Chemistry of Wood-Derived Biochars Using Wet Chemistry, Fourier Transform Infrared Spectroscopy and X-Ray Photoelectron Spectroscopy. *Soil Research* **2015**, *53* (7), 753−762.

(35) Tsechansky, L.; Graber, E. R. Methodological Limitations to Determining Acidic Groups at Biochar Surfaces via the Boehm Titration. *Carbon* **2014**, *66*, 730−733.

https://doi.org/10.1021/acssusresmgt.3c00104
ACS Sustainable Resour. Manage. 2024, 1, 707−720

(36) Trakal, L.; Veselská, V.; Šafařík, I.; Vítková, M.; Číhalová, S.; Komárek, M. Lead and Cadmium Sorption Mechanisms on Magnetically Modified Biochars. *Bioresource Technology* **2016**, *203*, 318−324.
(37) Güzel, F.; Sayğılı, H.; Akkaya Sayğılı, G.; Koyuncu, F.; Yılmaz, C. Optimal Oxidation with Nitric Acid of Biochar Derived from Pyrolysis of Weeds and Its Application in Removal of Hazardous Dye Methylene Blue from Aqueous Solution. *Journal of Cleaner Production* **2017**, *144*, 260−265.
(38) Xu, Y.; Bai, T.; Yan, Y.; Zhao, Y.; Yuan, L.; Pan, P.; Jiang, Z. Enhanced Removal of Hexavalent Chromium by Different Acid-Modified Biochar Derived from Corn Straw: Behavior and Mechanism. *Water Science and Technology* **2020**, *81* (10), 2270−2280.
(39) Li, M.; Liu, Q.; Lou, Z.; Wang, Y.; Zhang, Y.; Qian, G. Method To Characterize Acid-Base Behavior of Biochar: Site Modeling and Theoretical Simulation. *ACS Sustainable Chem. Eng.* **2014**, *2* (11), 2501−2509.
(40) Lawrinenko, M.; Laird, D. A. Anion Exchange Capacity of Biochar. *Green Chem.* **2015**, *17* (9), 4628−4636.
(41) Tipping, E.; Hurley, M. A. A Unifying Model of Cation Binding by Humic Substances. *Geochim. Cosmochim. Acta* **1992**, *56* (10), 3627−3641.
(42) Benedetti, M. F.; Van Riemsdijk, W. H.; Koopal, L. K. Humic Substances Considered as a Heterogeneous Donnan Gel Phase. *Environ. Sci. Technol.* **1996**, *30* (6), 1805−1813.
(43) Duval, J. F.; Wilkinson, K. I.; Van Leeuwen, H. P.; Buffle, J. Humic Substances are Soft and Permeable: Evidence from Their Electrophoretic Mobilities. *Environ. Sci. Technol.* **2005**, *39* (17), 6435−6445.
(44) Pinheiro, J. P.; Rotureau, E.; Duval, J. F. L. Addressing the Electrostatic Component of Protons Binding to Aquatic Nanoparticles Beyond the Non-Ideal Competitive Adsorption (NICA)-Donnan Level: Theory and Application to Analysis of Proton Titration Data for Humic Matter. *J. Colloid Interface Sci.* **2021**, *583*, 642−651.
(45) Lee, J. W.; Kidder, M.; Evans, B. R.; Paik, S.; Buchanan, A. C., 3rd; Garten, C. T.; Brown, R. C. Characterization of Biochars Produced from Cornstovers for Soil Amendment. *Environ. Sci. Technol.* **2010**, *44* (20), 7970−7974.
(46) van Beinum, W.; Hofmann, A.; Meeussen, J. C.; Kretzschmar, R. Sorption Kinetics of Strontium in Porous Hydrous Ferric Oxide Aggregates I. The Donnan Diffusion Model. *J. Colloid Interface Sci.* **2005**, *283* (1), 18−28.
(47) Biesheuvel, P. M.; Fu, Y.; Bazant, M. Z. Diffuse Charge and Faradaic Reactions in Porous Electrodes. *Phys. Rev. E* **2011**, *83* (6), 061507.
(48) Tan, Z.; Zou, J.; Zhang, L.; Huang, Q. Morphology, Pore Size Distribution, and Nutrient Characteristics in Biochars Under Different Pyrolysis Temperatures and Atmospheres. *Journal of Material Cycles and Waste Management* **2018**, *20* (2), 1036−1049.
(49) Huang, H.; Reddy, N. G.; Huang, X.; Chen, P.; Wang, P.; Zhang, Y.; Huang, Y.; Lin, P.; Garg, A. Effects of Pyrolysis Temperature, Feedstock Type and Compaction on Water Retention of Biochar Amended Soil. *Sci. Rep.* **2021**, *11* (1), 7419.
(50) Zhou, L.; Huang, Y.; Qiu, W.; Sun, Z.; Liu, Z.; Song, Z. Adsorption Properties of Nano-MnO_2-Biochar Composites for Copper in Aqueous Solution. *Molecules* **2017**, *22* (1), 173.
(51) Sun, K.; Kang, M.; Zhang, Z.; Jin, J.; Wang, Z.; Pan, Z.; Xu, D.; Wu, F.; Xing, B. Impact of Deashing Treatment on Biochar Structural Properties and Potential Sorption Mechanisms of Phenanthrene. *Environ. Sci. Technol.* **2013**, *47* (20), 11473−11481.
(52) Yang, F.; Zhang, Q.; Jian, H.; Wang, C.; Xing, B.; Sun, H.; Hao, Y. Effect of Biochar-Derived Dissolved Organic Matter on Adsorption of Sulfamethoxazole and Chloramphenicol. *Journal of Hazardous Materials* **2020**, *396*, 122598.
(53) Fidel, R. B.; Laird, D. A.; Thompson, M. L.; Lawrinenko, M. Characterization and Quantification of Biochar Alkalinity. *Chemosphere* **2017**, *167*, 367−373.
(54) Avena, M. J.; Koopal, L. K.; van Riemsdijk, W. H. Proton Binding to Humic Acids: Electrostatic and Intrinsic Interactions. *J. Colloid Interface Sci.* **1999**, *217* (1), 37−48.
(55) Kinniburgh, D. G.; van Riemsdijk, W. H.; Koopal, L. K.; Borkovec, M.; Benedetti, M. F.; Avena, M. J. Ion Binding to Natural Organic Matter: Competition, Heterogeneity, Stoichiometry and Thermodynamic Consistency. *Colloids Surf., A* **1999**, *151* (1-2), 147−166.
(56) Kinniburgh, D.; Tang, C. FIT User Guide, British Geological Survey; Keyworth, Great Britain, 1993.
(57) Keizer, M. G.; van Riemsdijk, W. H. *ECOSAT. A Computer Program for the Calculation of Speciation and Transport in Soil-Water Systems*, version 4.8; Wageningen University Department of Soil Quality: Wageningen, The Netherlands, 2007.
(58) Chen, T.; Zhang, Y.; Wang, H.; Lu, W.; Zhou, Z.; Zhang, Y.; Ren, L. Influence of Pyrolysis Temperature on Characteristics and Heavy Metal Adsorptive Performance of Biochar Derived from Municipal Sewage Sludge. *Bioresource Technology* **2014**, *164*, 47−54.
(59) Usman, A. R. A.; Abduljabbar, A.; Vithanage, M.; Ok, Y. S.; Ahmad, M.; Ahmad, M.; Elfaki, J.; Abdulazeem, S. S.; Al-Wabel, M. I. Biochar Production from Date Palm Waste: Charring Temperature Induced Changes in Composition and Surface Chemistry. *Journal of Analytical and Applied Pyrolysis* **2015**, *115*, 392−400.
(60) Zoroufchi Benis, K.; Motalebi Damuchali, A.; Soltan, J.; McPhedran, K. N. Treatment of Aqueous Arsenic - A Review of Biochar Modification Methods. *Science of The Total Environment* **2020**, *739*, 139750.
(61) Jin, J.; Li, S.; Peng, X.; Liu, W.; Zhang, C.; Yang, Y.; Han, L.; Du, Z.; Sun, K.; Wang, X. HNO_3 Modified Biochars for Uranium (VI) Removal from Aqueous Solution. *Bioresource Technology* **2018**, *256*, 247−253.
(62) Zeng, H.; Zeng, H.; Zhang, H.; Shahab, A.; Zhang, K.; Lu, Y.; Nabi, I.; Naseem, F.; Ullah, H. Efficient Adsorption of Cr (VI) from Aqueous Environments by Phosphoric Acid Activated Eucalyptus Biochar. *Journal of Cleaner Production* **2021**, *286*, 124964.
(63) He, X.; Hong, Z. N.; Shi, R. Y.; Cui, J. Q.; Lai, H. W.; Lu, H. L.; Xu, R. K. The Effects of H_2O_2- and HNO_3/H_2SO_4-Modified Biochars on the Resistance of Acid Paddy Soil to Acidification. *Environmental Pollution* **2022**, *293*, 118588.
(64) Olk, D. C.; Bloom, P. R.; Perdue, E. M.; McKnight, D. M.; Chen, Y.; Farenhorst, A.; Senesi, N.; Chin, Y. P.; Schmitt-Kopplin, P.; Hertkorn, N.; Harir, M. Environmental and Agricultural Relevance of Humic Fractions Extracted by Alkali from Soils and Natural Waters. *Journal of Environmental Quality* **2019**, *48* (2), 217−232.
(65) Keiluweit, M.; Nico, P. S.; Johnson, M. G.; Kleber, M. Dynamic Molecular Structure of Plant Biomass-Derived Black Carbon (Biochar). *Environ. Sci. Technol.* **2010**, *44* (4), 1247−1253.
(66) Leng, L.; Xiong, Q.; Yang, L.; Li, H.; Zhou, Y.; Zhang, W.; Jiang, S.; Li, H.; Huang, H. An Overview on Engineering the Surface Area and Porosity of Biochar. *Science of The Total Environment* **2021**, *763*, 144204.
(67) Xiong, J.; Zhou, M.; Qu, C.; Yu, D.; Chen, C.; Wang, M.; Tan, W. Quantitative Analysis of Pb Adsorption on Sulfhydryl-Modified Biochar. *Biochar* **2021**, *3* (1), 37−49.
(68) Fang, Q.; Chen, B.; Lin, Y.; Guan, Y. Aromatic and Hydrophobic Surfaces of Wood-Derived Biochar Enhance Perchlorate Adsorption via Hydrogen Bonding to Oxygen-Containing Organic Groups. *Environ. Sci. Technol.* **2014**, *48* (1), 279−288.
(69) Xiao, X.; Chen, B. A Direct Observation of the Fine Aromatic Clusters and Molecular Structures of Biochars. *Environ. Sci. Technol.* **2017**, *51* (10), 5473−5482.
(70) Yazdani, M. R.; Duimovich, N.; Tiraferri, A.; Laurell, P.; Borghei, M.; Zimmerman, J. B.; Vahala, R. Tailored Mesoporous Biochar Sorbents from Pinecone Biomass for the Adsorption of Natural Organic Matter from Lake Water. *Journal of Molecular Liquids* **2019**, *291*, 111248.
(71) Lenoir, T.; Manceau, A. Number of Independent Parameters in the Potentiometric Titration of Humic Substances. *Langmuir* **2010**, *26* (6), 3998−4003.

https://doi.org/10.1021/acssusresmgt.3c00104
ACS Sustainable Resour. Manage. 2024, 1, 707−720

(72) Janot, N.; Pinheiro, J. P.; Botero, W. G.; Meeussen, J. C. L.; Groenenberg, J. E. PEST-ORCHESTRA, A Tool for Optimising Advanced Ion-Binding Model Parameters: Derivation of NICA-Donnan Model Parameters for Humic Substances Reactivity. *Environmental Chemistry* **2017**, *14* (1), 31.
(73) Fest, E. P. M. J.; Temminghoff, E. J. M.; Griffioen, J.; Van Riemsdijk, W. H. Proton Buffering and Metal Leaching in Sandy Soils. *Environ. Sci. Technol.* **2005**, *39* (20), 7901−7908.
(74) Groenenberg, J. E.; Lofts, S. The Use of Assemblage Models to Describe Trace Element Partitioning, Speciation, and Fate: A Review. *Environmental Toxicology and Chemistry* **2014**, *33* (10), 2181−2196.
(75) Weng, L.; Temminghoff, E. J.; Van Riemsdijk, W. H. Contribution of Individual Sorbents to the Control of Heavy Metal Activity in Sandy Soil. *Environ. Sci. Technol.* **2001**, *35* (22), 4436−4443.
(76) Gao, H.; Koopmans, G. F.; Song, J.; Groenenberg, J. E.; Liu, X.; Comans, R. N. J.; Weng, L. Evaluation of Heavy Metal Availability in Soils Near Former Zinc Smelters by Chemical Extractions and Geochemical Modelling. *Geoderma* **2022**, *423*, 115970.
(77) Römkens, P. F.; Guo, H.-Y.; Chu, C.-L.; Liu, T.-S.; Chiang, C.-F.; Koopmans, G. F. Characterization of Soil Heavy Metal Pools in Paddy Fields in Taiwan: Chemical Extraction and Solid-Solution Partitioning. *Journal of Soils and Sediments* **2009**, *9* (3), 216−228.
(78) Sharma, P. K.; Kumar, R.; Singh, R. K.; Sharma, P.; Ghosh, A. Review on Arsenic Removal Using Biochar-Based Materials. *Groundwater for Sustainable Development* **2022**, *17*, 100740.
(79) Fageria, N.; Baligar, V.; Clark, R. Micronutrients in Crop Production. *Advances in agronomy* **2002**, *77*, 185−268.
(80) Wu, P.; Cui, P.-X.; Fang, G.-D.; Wang, Y.; Wang, S.-Q.; Zhou, D.-M.; Zhang, W.; Wang, Y.-J. Biochar Decreased the Bioavailability of Zn to Rice and Wheat Grains: Insights from Microscopic to Macroscopic Scales. *Science of The Total Environment* **2018**, *621*, 160−167.
(81) Xu, Q.; Xu, Q.; Zhu, H.; Li, H.; Yin, W.; Feng, K.; Wang, S.; Wang, X. Does Biochar Application in Heavy Metal-Contaminated Soils Affect Soil Micronutrient Dynamics? *Chemosphere* **2022**, *290*, 133349.
(82) Luo, D.; Wang, L.; Nan, H.; Cao, Y.; Wang, H.; Kumar, T. V.; Wang, C. Phosphorus Adsorption by Functionalized Biochar: A Review. *Environmental Chemistry Letters* **2023**, *21* (1), 497−524.
(83) Munar-Florez, D. A.; Varón-Cardenas, D. A.; Ramírez-Contreras, N. E.; García-Núñez, J. A. Adsorption of Ammonium and Phosphates by Biochar Produced from Oil Palm Shells: Effects of Production Conditions. *Results in Chemistry* **2021**, *3*, 100119.
(84) Bilias, F.; Kalderis, D.; Richardson, C.; Barbayiannis, N.; Gasparatos, D. Biochar Application as a Soil Potassium Management Strategy: A Review. *Science of The Total Environment* **2023**, *858*, 159782.

https://doi.org/10.1021/acssusresmgt.3c00104
ACS Sustainable Resour. Manage. 2024, 1, 707−720